OTHR Impulsive Interference Detection based on AR Model in Phase Domain

TAO LIU, JIE WANG
Electronic Engineering College
the University of Electronic Science and Technology of China
Chengdu, 610054
CHINA
open-tony@163.com

Abstract: - Based on autoregression(AR) model in phase domain, this paper proposes a novel impulsive interference(IMI) detection algorithm for over-the-horizon radar. This is achieved by regarding IMI phase spectrum as complex sinusoid signal and modeling it by AR model. Then we can take the full advantage of the sinusoid signal estimation algorithm. After getting zeros of AR model transfer function, the amount of the contained sinusoid signals and their frequency parameters can be estimated. The angular value of zero is exactly corresponding to IMI position of interest. Details and improvements are also discussed in this paper. This algorithm's operational performance is evaluated using experimental data sets collected from a high frequency surface wave (HFSW) OTHR system, and is proved to be suitable for most types of IMIs.

Key-Words: - Autoregression Model, Impulsive Interference, Interference Detection, Over-the-horizon Radar, Phase Spectrum

1 Introduction

Over-the-horizon radar regularly operates in high frequency(HF) band(3-30MHz) and utilizes linear frequency modulated continuous waveform(FMCW) processing. OTHR has the attractive ability of radiation propagation beyond the line-of-sight, either by ground-waves diffracted around the earth curvature or by sky-waves refracted by the ionosphere[1]. The former propagation, referred to as ground-wave or surface-wave OTHR, can see over the horizon of 200-300km, whereas the latter see up to 1000-3000km. Both are widely used for ocean state remote sensing, marine ships and aircrafts detection in both military and civilian applications[2-6].

HF OTHR works in a very crowded electromagnetic environment mainly due to the rapid development of human short-wave communication and other electromagnetic applications. HF band is now so crowded that unoccupied clean frequency channel with sufficient bandwidth(50-100kHz) is extremely difficult to find[7,8].

Meanwhile, OTHR works in a very complicated environment which brings significant impact on radar sensitivity, mainly resulted from both strong clutter and impulsive interference (IMI). Firstly, the echo signal is mixed with strong ocean and ground clutter. Ground clutter, mainly caused by backscattering from ground surfaces, exhibits regularly as narrow-band signal with Doppler frequency close to zero-Herz, which can be modeled as constant in temporal echo. The ocean clutter is usually modeled as two Bragg peaks for first-order scattering and surrounding continuum for high-order scattering, where both scatterings are the selective reaction of electromagnetic wave and ocean currency wave[9]. The Bragg peaks usually have amplitudes of two orders of magnitude higher than those of the surrounding continuum[8]. Secondly, OTHR operations regularly experience shortfalls in performance particularly in the presence of external IMIs. Typical external IMI may be either natural or man-make sources, including the echo of meteor trail from the universe [10][11] [12], the lightning in the air[13], the shortwave radio communication electromagnetic wave interference[8]. IMIs are usually 20-40dB stronger than the thermal noise of receiver[14]. Each IMI deposits high-amplitude broadband noise energy in the Doppler spectrum. IMIs typically mask the entire range-Doppler search space and is characterized by wider bandwidth, short duration and complicated spectrum structures. For example, the physics of lightning IMI indicates total impulse durations lasting 200 to 400ms. Therefore, the continuous coherent processing interval(CPI) of 2 to 4 seconds typically used for aircraft detection are quite vulnerable to IMIs. This may reduce the radar sensitivity on the order of 10dB, making it unacceptable to track small aircraft[13].

Meteor trail echo is a kind of backscatter signal that is transmitted from the transmitter and reflected by the meteor trail body. Its duration is proportional to the mass of the meteor body, typically hundreds of milliseconds to several seconds, for example between 0.188s to 2.5935s[10]. Lightning impulse rates of one per second to one per 5 seconds are typical during active storms, and the physics of lightning indicates total impulse durations lasting 200 to 400ms[13]. Short-wave radio communication, such as broadcast station and communication station, is a kind of man-made interference source. The radio station has the repetition period asynchronous with that of OTHR. Short-wave communication signal is normally single-side amplitude modulated. When through the receiver, its equivalent bandwidth is equal to that of the receiver[15].

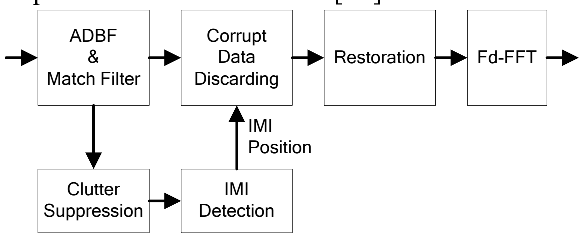

Fig.1 Block Diagram of Typical IMI Detection and Suppression

While the problem of IMI effects on OTHR performance have been noted for many years, not until recently could a set of detection and suppression algorithms using advanced digital signal processing algorithms be proposed and implemented in radar operations depending on hardware with high computational performance. Figure 1 illustrates a block diagram of typical IMI detection and suppression processing, where a key part is the IMI detection. “Clutter suppression” first suppresses clutter in the original temporal data from adaptive digital beamforming(ADBF) and match filter, corresponding to a certain range bin; “IMI Detection unit” detects and estimates the IMI position; “Corrupt Data Discarding” deletes the corrupt data segment where IMI exists; “Restoration” restores the corrupt segment by using linear prediction and estimating data from the neighboring good data samples for the purpose of keeping the continuity and coherency of data; then the data is processed by “Fd-FFT” to extract the Doppler information. From the viewpoint of interference suppression, the IMI Detection is a key step to the next processing.

Some proposals for IMI detection and suppression has been reported[7,8,11-13,16-21]. Fabrizio focuses on spatial processing, and proposes a set of SAP and STAP algorithms[7,8,17-19]. Huang[20] and Xin[21] adopt wavelet singular detection method and amplitude threshold method respectively for IMI detection. In these methods, the processing depends greatly on the costly clutter suppression, or must selectively utilize the secondary data without clutter as in [7,8].

In [4] Barnum directly masked the clutter Doppler bins to zero, and took IFFT to transform back to time domain. After that, the IMI can be detected by means of RMS threshold updated at every sample within CPI. Barnum’s algorithm is simple to implement. However, it uses an ideal high-pass filter without transitional region to mask the Doppler bins, leading to long temporal trail with higher amplitude. As a result, if one IMI has significantly higher amplitude than other IMI-s, the long trail from this dominant IMI peak will extend to almost the whole CPI, submerging the peaks for other IMI-s. This would make the IMI-s with lower amplitudes effectively undetectable. This effect is illustrated by Fig.2, where a dominant IMI is at 110-th sweep and two minor at 25-th and 90-th respectively. Two minor IMIs are almost invisible in the figure, and undetectable through threshold examination.

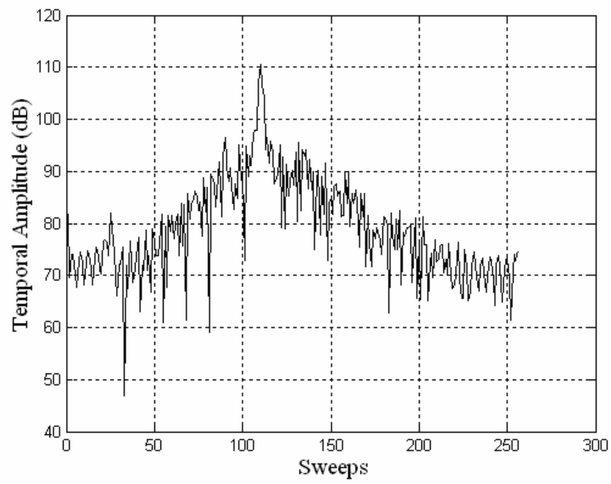

Fig.2 Processed Result by Barnum’s Method

This paper proposes a novel IMI detection algorithm based on phase-domain AR model while. It is known that the AR model is usually used for temporal signal modeling, where the basis is extended to phase-domain in this paper. This paper firstly analyzes the characteristics of IMI Doppler spectrum, and models its phase spectrum as complex sinusoid signal. Based on this consideration, every IMI's phase spectrum can be modeled by AR model. The zeros of AR model transfer function exclusively capture the information on the IMI amount and position. This proposed algorithm need a pre-processing including DFT and clutter suppression. Its operational performance is evaluated using experimental data from a HFSW OTHR system, indicating that this proposed algorithm works efficiently and is suitable for most types of IMIs. In this paper, we do not consider spatial processing and restrict the attention to temporal only, that is to say, the data objects are the output of beamforming and denoted as a function of time.

This paper experimentally extends the application of AR modeling from time domain to phase domain, from targets signals estimation to interference. This also finds a way of estimating IMIs by means of sinusoid signal estimation, that is, any sinusoid estimation method for conventional target signal can also theoretically be utilized here for IMI, such as MUSIC or ESPRIT.

This paper is organized as follows. The signal model is constructed in Section 2, after which the proposed detection algorithm steps are described in Section 3. The experimental results are shown in Section 4. Conclusions are given in Section 5.

2 Signal Model

2.1 Radar Echo Model

Suppose that the radar transmits a burst of P coherent pulses in a CPI. OTHR has an antenna array with N elements corresponding to N reception channels. For every channel, the received signal is processed by amplification, filtering, A/D sampling, conversion to baseband and pulse compression respectively. The antenna beam is steered to a few directions covering the surveillance area. In one spatial beam, all data from N channels are combined to produce a complex range-sweep matrix with P-row and L-column. L is the number of range bins and P is the number of coherent pulses or range sweeps in a CPI. Every column has P samples, corresponding to a certain range. The FFT (Fd-FFT), or coherent integration, is then performed on every column and converts the range-sweep matrix into range-Doppler one. For every matrix element, a threshold decision is carried out. If the detection is declared in a particular range-Doppler cell, the target is implicitly assigned a direction that coincides with the steer direction of this beam.

A column of P scalar echo samples at a certain azimuth-range cell in one CPI can be modeled as

$$r(t) = s(t) + c(t) + i(t) + w(t) \qquad t = 0, \cdots, P-1 \tag{1}$$

where $s(t)$ is the target signal of interest, $c(t)$ is the ocean and ground clutter, $i(t)$ is the external IMI, $w(t)$ is the internal thermal noise assumed as white and weak. An ideal target of constant reflectivity and radial velocity over the CPI is modeled as a complex sinusoid signal:

$$s(t) = A_s e^{j\omega_d t} \tag{2}$$

where $\omega_d = 2\pi f_d$ is the Doppler frequency of target.

The dominant spectral components of OTHR ocean clutter is modeled as two complex sinusoid signals, whereas the high-order continuum is ignored[8]. The ground clutter has a very strong zero-Herz component and can be modeled as complex number. Therefore, the clutter component is modeled as

$$c(t) = c_a e^{j(\omega_c + \omega_B)t} + c_r e^{j(\omega_c - \omega_B)t} + c_g \tag{3}$$

where $\omega_B = 2\pi f_B$ is the Bragg frequency, $\omega_c = 2\pi f_c$ is the Doppler frequency corresponding to the ocean currency velocity, c_a and c_r are the advance and recede first-order ocean clutter amplitudes respectively, c_g is the ground clutter amplitude. Because the ocean currency radial velocity is low and changes slowly along time, the Doppler frequency ω_c is very small compared with Bragg frequency ω_B, and regarded as approximately constant over the whole CPI.

The external IMI is usually regarded as an impulse due to the short duration compared with CPI. As the main concern of this paper is to determine the position of the external interference, it is modeled as a Dirac function $\delta(t - t_0)$ with amplitude A_i, and position parameter t_0 that is exactly the aim of interest of this algorithm.

So the echo sample in (1) is rewritten as

$$\begin{aligned} r(t) &= c_a e^{j(\omega_c + \omega_B)t} + c_r e^{j(\omega_c - \omega_B)t} + c_g \\ &+ A_s e^{j\omega_d t} + A_i \delta(t - t_0) + w(t) \\ & t = 0, \cdots, P-1 \end{aligned} \tag{4}$$

2.2 Pseudo-target and Pseudo-noise

The solution to IMI detection problem in (4) is to identify the existence of $\delta(\;)$ and estimate its parameter t_0 . Let us look at the spectrum of the echo in (4), which can be expressed as:

$$R(\omega)=c_a\delta(\omega-\omega_c-\omega_B)+c_r\delta(\omega-\omega_c+\omega_B) \\ +c_g\delta(\omega)+\delta(\omega-\omega_d)+A_ie^{j\omega t_0}+W(\omega) \quad (5)$$

where $c_a\delta(\omega-\omega_c-\omega_B)+c_r\delta(\omega-\omega_c+\omega_B)$ is the spectrum of ocean clutter, $c_g\delta(\omega)$ spectrum of ground clutter, $\delta(\omega-\omega_d)$ spectrum of target signal, $A_ie^{j\omega t_0}$ spectrum of external IMI, $W(\omega)$ spectrum of noise which is very weak and approximately close to constant.

Make the variable substitution as

$$\omega\rightarrow t', \qquad t\rightarrow\omega'$$

So, (5) can be expressed as

$$R(t')=c_a\delta(t'-t_c'-t_B')+c_r\delta(t'-t_c'+t') \\ +c_g\delta(t')+\delta(t'-t_d')+A_ie^{j\omega_0't'}+W(t) \quad (6)$$

The equation (5) is entirely identical to (6) except for the variable symbol representing. Signal in (6) may be regarded as in a new "time domain". Components with $\delta(\ )$ representation and the last component $W(t)$ in (6) are all viewed as noise in the "time domain", referred to as pseudo-noise. The complex sinusoid signal $A_ie^{j\omega_0't'}$ is the "target signal of interest" or pseudo-target with "frequency" ω_0'. This sinusoid can be modeled by AR modeling method, and its detection and parameter estimation is a typical temporal sinusoid frequency estimation problem. When there are more IMIs than one, (6) can be generalized to have sum of complex sinusoid components $\sum_k A_{ik}e^{j\omega_k'n'}$ with different "frequencies" ω_k'. The sinusoid frequency estimation algorithm can still work perfectly.

Define the pseudo-signal-to-noise-ratio as

$$SNR'=\frac{S'}{N'}$$

where S' is the power of pseudo-target or IMI, N' is the power of other components in (6). When the SNR' is high enough, the frequency estimation algorithm can separate multiple sinusoid signal and estimate their corresponding frequency that declares the existence of IMI.

In fact, the frequency estimation algorithm in the new "time domain" is applied in the phase domain. The estimated "frequency" or pseudo-frequency is just on the original time domain. The pseudo-frequency just indicates the temporal position of IMIs. That is to say, the "frequency spectrum" of the frequency spectrum is just the time waveform. This fact can be comprehended through space transformation theory. Fourier transformation (FT) performs a kind of space transformation from one space to another. Generalized, the source space and the target one can be any linear space, either the time or the frequency space. So FT on the frequency space is reasonable and feasible, where the FT result is the time-reversed replica of original time waveform.

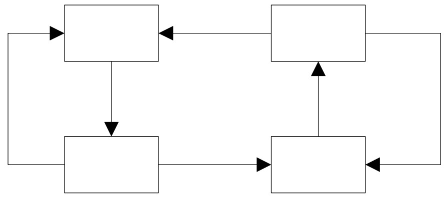

Fig.3 Transformation Relation of DFT and IDFT

The derivation can be briefly performed only on DFT. Fig.2 can explain the transformation relation, where we ignore the influence of factor N or 1/N. According to classical DFT:

$$x(n)=\frac{1}{N}\sum_{n=0}^{N-1}X(k)W_N^{-nk}$$

$$X(k)=\sum_{n=0}^{N-1}x(n)W_N^{nk}$$

$$W_n=e^{-j2\pi/N}$$

Make the variable substitution as $n=-m$, and we take

$$x(m)=x(-n)=\frac{1}{N}\sum_{n=0}^{N-1}X(k)W_N^{mk}$$

So, applying DFT on the frequency spectrum samples $X(k)$ can get $x(m)$, namely the time-reversed replica of $x(n)$. Consequently, when we use traditional temporal frequency estimation algorithms on frequency spectrum samples $X(k)$, we must make an extra time-reversion operation on the estimated pseudo-frequency.

2.3 AR Model and Frequency Estimation

The AR model fitting and frequency estimation for IMI method proposed in this paper is derived from the research work of Khan[9].

It is noted that, at high signal-to-noise ratio (SNR), linear prediction(LP), or autoregression (AR) based methods can be effectively utilized to estimate the frequencies of sinusoid signals. According to the principle of AR parametric model, the value $\tilde{x}(k)$ at any time instance k can be predicted as a weighted sum of L known values prior to k:

$$\tilde{x}(k) = -\sum_{i=1}^{L} x(k-i)\cdot a_i \qquad (7)$$

where, L is the order of the prediction filter, and $\{a_i\}_{i=1,2,\cdots L}$ are the prediction coefficients.

The prediction-error filter (PEF) calculates the difference between the predicted signal value and the actual signal value. If the signal fits this parametric model, then the output of the PEF is close to zero. When these prediction coefficients $\{a_i\}_{i=1,2,\cdots L}$ are used in a PEF, the transfer function can be written as :

$$H(z) = 1 + \sum_{i=1}^{L} a_i z^{-i} \qquad (8)$$

According to the transfer function, it is known that this PEF is an all-zero filter. For a signal mixed with M complex sinusoids, the transfer function has M zeros located on the unit circle at the angular positions corresponding to the frequencies of these M sinusoids. If the transfer function has L zeros, where L>M, then the L-M extraneous zeros are uniformly distributed inside of the unit circle.

To effectively extract the sinusoid at every position and provide an estimation with higher confidence level, the coefficients of the PEF must be estimated using very short data segments. A famous AR modeling method is implemented based on the forward-backward linear prediction (FBLP) method[16]. This is a robust technique which estimate the PEF coefficients by minimizing the prediction errors both in the forward and backward directions. For a signal vector x(k), k=1,2,…N, and a prediction order L, the prediction coefficients may be estimated by solving the following system of linear equation:

$$Aa = -b \qquad (9)$$

$$A = \begin{bmatrix} x(L) & x(L-1) & \cdots & x(1) \\ x(L+1) & x(L) & \cdots & x(2) \\ \vdots & \vdots & \vdots & \vdots \\ x(N-1) & x(N-2) & \cdots & x(N-L) \\ x^*(2) & x^*(3) & \cdots & x^*(L+1) \\ \vdots & \vdots & \vdots & \vdots \\ x^*(N-L+1) & x^*(N-L+2) & \cdots & x^*(N) \end{bmatrix}$$

$$a = [a_1, a_2, \cdots a_L]^T$$

$$b = [x(L+1), x(L+2), \cdots, x(N), x^*(1), \cdots, x^*(N-L)]^T$$

3 Detection Algorithm based on AR model in phase domain

3.1 Pseudo-Target Estimation by AR Model

Besides DFT, we can use other frequency estimation methods for the purpose of target detection. Here, the AR modeling is an optional one. Its PEF properties can be used to detect the pseudo-target or IMI: A short frame of data in new "time domain" is applied for the AR modeling; then the number of zeros of the PEF on the unit circle determines the number of sinusoids or IMIs in the signal, and the angular φ of each zero determines each IMI position t, where the map relation is

$$\varphi \in [0, 2\pi) \mapsto t \in [0, P) \qquad (10)$$

According to analysis on DFT in Fig.3, the pseudo-frequency must be time-reversed to original time domain. Or we can perform an equivalent conjugation operation on the zeros of equation (8).

3.2 Estimations on PEF Coefficients

Equation (9) is generally over-determined and a typical least-squared (LS) solution is suitable. This is the first and immediate solution to PEF coefficients estimation.

$$a = -\left(A^H A\right)^{-1} A^H \cdot b \qquad (11)$$

Alternatively, the coefficients can be estimated iteratively in an adaptive mode. Based on the scheme in [9], this paper utilizes an adaptive filter scheme whose block diagram is shown in Fig.1. The input signal into adaptive filter is the data samples in Doppler domain, which is quite different from that in [9]. The iterative update was implemented using the SPNLMS [23], which is derived from the famous LMS algorithm[24]. The filter coefficients are updated for each input sample, according to the following:

$$A(k+1) = A(k) + \frac{2\mu \cdot e(k)\cdot X(k)}{(L+1)\cdot[\sigma(k)]^2} \qquad (13)$$

$$[\sigma(k)]^2 = \alpha\cdot[x(k)]^2 + (1-\alpha)\cdot[\sigma(k-1)]^2$$

$$A(k) = [a_1(k), a_2(k), \cdots a_L(k)]^T$$

$$X(k) = [x(k), x(k-1), \cdots x(k-L)]^T$$

$$0 < \mu < 1, \quad 0 < \alpha \ll 1$$

Its adaptation performance is controlled by the convergence parameter μ and the "forgetting" factor α. The former must be matched to the signal statistics: too large will lead to slow convergence, whereas too small may lead to significant lagging behind the rapid changing signal statistics. The factor α is participating in the exponentially weighted sum of the past values of x(k), and their effect becomes negligible after an interval of about 1/α samples.

These two scheme of estimation on coefficients are both tested by sets of experimental data and illustrated in the following section.

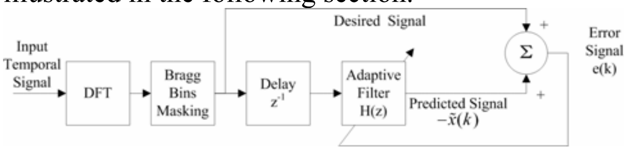

Fig.4 Block Diagram of Adaptive Iteration for Coefficients Estimation

3.3 Clutter Suppression

Unfortunately, in practical operations, the power N' is regularly higher than S' due to the energy of clutter far higher than that of IMI, which causes the SNR' lower and AR modeling fail. An intuitive solution is to suppress clutter prior to the AR modeling.

Typical clutter suppression algorithms with perfect performance are usually characterized by high computational cost. For example, the iteration-cancellation method is described in [22]. Each short-time complex Doppler spectrum (at each range and azimuth) is operated upon separately, and then the clutter cancellation proceeds by iterations. At each iteration, the largest remaining Doppler peak (usually clutter) is modeled as a sinusoid(actually a complex exponential)and subtracted. Another method based on generalized MTI filter is described in [21], where the MTI is based on the subspace projection and filtering. The method with generalized MTI has a disadvantage of eigen-decomposition on large-size covariance matrix.

By virtue of clutter characteristics described in (3), Barnum proposes an extremely simple clutter suppression method[13]. The Doppler bins ranging are directly masked or set to zero for the purpose of filtering out dominant clutter energy, that is, the ground clutter and the first-order ocean clutter.

Three schemes of clutter suppression are tested and compared in this paper. Although Barnum's simple masking may cause long temporal trail as analyzed in Section 1, experiments shows that this shortage brings little impact on the detection results.

3.4 Zeros Clustering

All zeros are illustrated in the zero-pole map, where some groups will be clustered obviously and compactly on the unit circle as shown in the following experimental result. Cluster center will give a proper mean estimation among these closely surrounding zeros. The well-known cluster algorithms can be used to estimate the cluster center such as K-mean and ISODATA[25]. The former is modified a little and utilized in this paper for zeros clustering. Its steps are described briefly as follow:

1) All zeros with amplitude before 1.1 and below 0.8 is discarded

2) Initially, select the first zero into the set C_1, and other zeros stayed in the un-clustered set C_0

3) Select one zero z from C_0, calculate the minimum distance

$$d = \min_{\substack{k>0 \\ z\in C_0}} D_E\left(z, C_k\right)$$

where $D_E\left(z, C_k\right)$ is the Euclidian distance from z to center of C_k. If $d > d_{th}$, then z will be moved from C_0 into a new set $C_N, N > 0$ as its first element, or z will be moved into its nearest cluster

4) Continue 3) until C_0 is empty.

5) Cluster with element amount less than η will be discarded as a false cluster.

6) Amount of remained cluster indicates the amount of potential IMIs, and the cluster centers are the IMI positions.

Here, the threshold d_{th} is a key factor which will significantly influence the clustered amount and center. There is no other a prior information for it, and we can only uses experimental statistics value. The statistics distribution will be illustrated in the following experimental results section.

3.5 Algorithm Steps

According to the above analysis, the proposed algorithm step is described as:

1) Perform the DFT or FFT on the echo r(t) in (1);

2) Clutter Suppression;

3) Extract a frame of N samples from the frequency spectrum and apply them to (11) or (12) to get the AR coefficients $\{a_i\}_{i=1,2,\cdots L}$

4) Fill the AR coefficients to the transfer function of the PEF and calculate its zeros according to (8)

5) Move to the next starting position of frame and go back to step 3) until the frame ending position is exceeding over the last sample

6) Plot all zeros derived from step 4) in the zero-pole map, and the clustering zeros in the unit circle indicate an IMI and the angular position is mapped back to temporal sampling position.

3.6 Improvements

A number of experimental data set shows that through this proposed algorithm, there is always a false zero at the last sample position as shown in next section. Deep analysis on the algorithm derivation indicates that it is arising due to the discontinuity on the boundary. Specifically, when we perform the DFT or FFT on the temporal data segment of P samples, we implicitly impose a periodic expanding on this segment. The discontinuity at the boundary between one segment and the next one is almost inevitable. This discontinuity leads to the unexpected false zero.

To solve this problem, we propose a method of symmetrical periodic expanding before DFT

$$R(\omega)=\begin{cases} R(\omega), 0<\omega<P-1 \\ R(-\omega), P<\omega<2P-1 \end{cases}$$

Correspondingly, the mapping relation (10) will be

$$\varphi \in [0,2\pi) \mapsto t \in [0,2P)$$

After this improvement, there will exist two set of symmetrical zeros on both side of real axis of unit circle. But the unexpected false zero has disappeared.

4 Experimental Results

4.1 Data Collection

The algorithm described above is tested using experimental data collected from a real bistatic HF OTHR system in China. The receiving system is based on ULA of vertical monopole antenna elements. The isolation between transmit and receive sites permits bistatic operation with a linear FMCW. Experimental data were collected in a research for IMI suppression on OTHR during which the interference type was unknown and possibly arose due to a multiplicity of man-made and natural sources. Total over hundred groups of data are collected, from which nine groups are selected for research on IMI suppression based on this proposed algorithm. Each CPI consists of P=256 linear FMCW pulses or sweeps with center frequency determined in real-time by the frequency management system.

4.2 Zero-pole Maps Results

Four groups of temporal echo samples corresponding to four azimuth-range cells are participating in the experimental verification. Fig.5 - Fig.8 illustrate their processed results by means of zero-pole maps. The first three tests use LS solution (11) with N = 20 and L = 6 for AR model coefficients estimation, but with different clutter suppression method. The fourth group uses adaptive scheme in Fig.4 for AR model coefficients estimation.

In all four figures, there are zeros clusters obviously located on the unit circle, and other zeros are distributed randomly inside the unit circle. According to the above analysis, these obvious clusters may potentially correspond to IMIs.

Fig.5 shows the zero-pole map for the first group of data. In its processing, the simple clutter masking to zero-value as in [13] is adopted. Fig.5 illustrates obviously three group of clustered zeros located on the unit circle, at angular of about 30^0, 160^0 and 0^0 respectively. These three positions correspond to three potential IMI positions. For the purpose of verification on estimated positions, we view with the naked eye on the temporal waveform. It is concluded that the first two positions are exactly true estimations, but the last one at 0^0 is a false one.

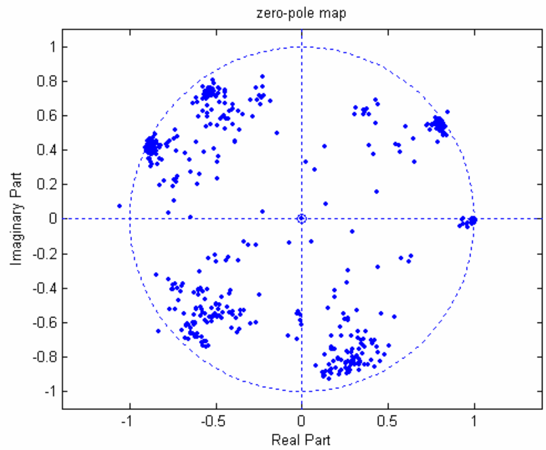

Fig.5 Zero-pole Map for 1st Group Data

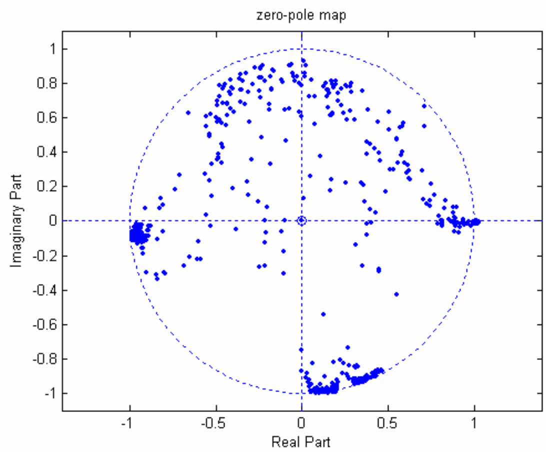

Fig.6 Zero-pole Map for 2nd Group Data

Fig.6 shows the zero-pole map for the second group of data. The iterative cancellation in [22] is adopted here. Fig.3 also illustrates obviously four group of clustered zeros located on the unit circle, at angular of about 185^0, 270^0, 290^0 and 0^0 respectively. These first three are perfect estimations with high confidence level. But last one at 0^0 is also a false one.

Fig.7 is corresponding to the third group, and uses the general MTI for clutter suppression as in [21]. It also has a false estimation at 0^o as in Fig.5 and Fig.6. Here, Fig.7 illustrates three reliable estimations for IMI positions. From results in Fig.5 - Fig.7, it is obvious that the proposed algorithm can work perfectly with simple and complicated clutter suppression, but Fig.5 has a lower computational cost and consequently is preferred.

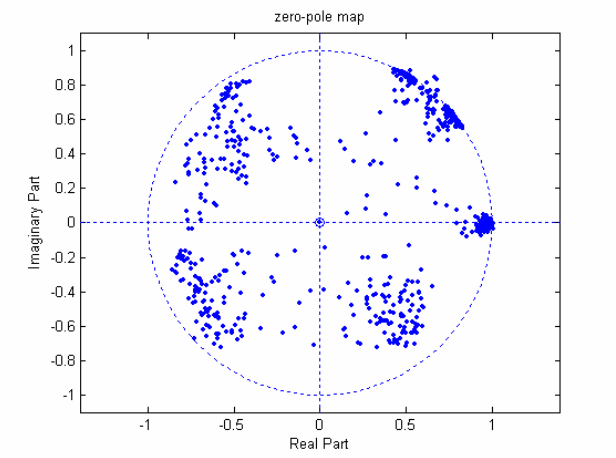

Fig.7 Zero-pole Map for 3rd Group Data

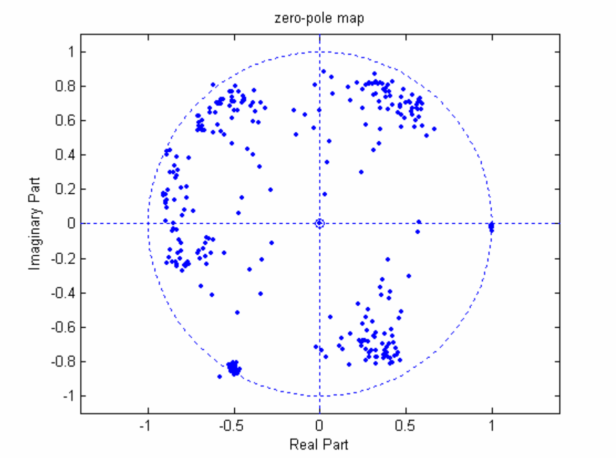

Fig.8 Zero-pole Map for 2nd Group Data

Fig.8 is for the 4th group. It uses the simple clutter masking as in [13] and the adaptive iterative scheme for coefficients estimation as shown in Fig.4. It also has false estimation at 0^o $ and should be discarded manually. From comparison between Fig.5 and Fig.8, both LS and adaptive scheme has perfect performance on parameter estimation.

4.3 Angular Mapping into Temporal Position

For the purpose of identify the position of IMIs as a function of temporal position rather than angular, the angular value of zero is calculated and mapped into temporal sample position or sweep according to (10). Fig.9 shows the temporal position map corresponding to zeros in Fig.5. All zeros with amplitude less than 0.9 is regarded as non-IMI and discarded. From this figure, zeros at 30^0 and 160^0 are corresponding to temporal of 25-th and 110-th sweep. Zero at 0^0 corresponding to 1-th or 255-th sweep, namely the boundary, is the false one.

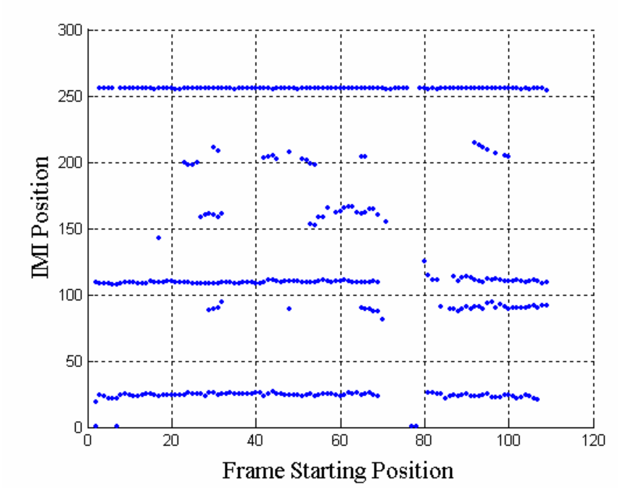

Fig.9 Temporal Position of Estimated IMIs, for 1st Group Data

4.4 False Cluster Rejection

Through many groups of other experimental data, it is demonstrated that there is always a cluster of zeros centered at 0^0 position. According to the analysis on 3.6, these are all false IMIs, arising from the discontinuity of boundary when processing DFT. All false estimations at 0^o should be discarded manually. But when a true IMI located near 0^0, it is hard to discriminate true or false. To solve this problem, Section 3.6 proposes a solution of symmetrical periodic expanding, through which these 1st group data are processed and shown in Fig.10. The false estimation at 0^o has been entirely discarded automatically. It still uses N = 20 and L = 6 for AR model.

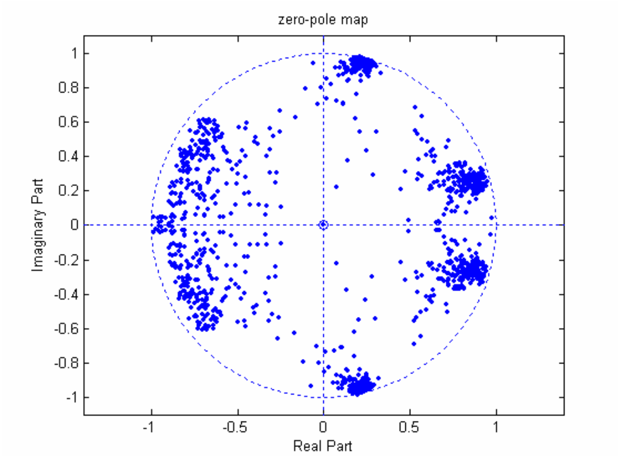

Fig.10 Zero-pole map for symmetrical periodic expanding 1st group data

4.5 Impact from PEF Order

To LS fitting in (11), we must select a proper PEF order. If the order is small than the true amount of IMIs, at most L/2 clusters will be illustrated in zero-pole map. If the order is too large, it will result in extra unexpected zeros close to unit circle boundary. This phenomenon is demonstrated in Fig.5, Fig.10 and Fig.11, where these three has different order L for same 1st group data. In Fig.10, the order is 4, and consequently there is obviously two clutters. In Fig.11, the order is 10. It not only has shown a same cluster positions as Fig.5 and Fig.10, but also a new position at 130^0. Unfortunately, there are other unexpected zeros loosely distributed from 180^0 to 360^0.

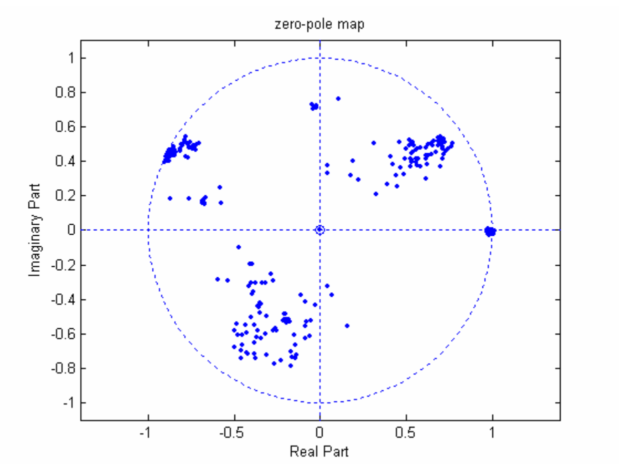

Fig.10 Effect of different PEF order, with order L=4

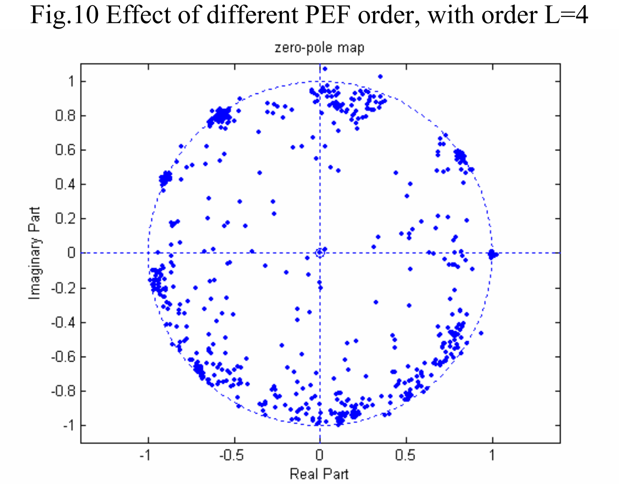

Fig.11 Effect of different PEF order, with order L=8

4.6 Statistics Properties of Cluster

According to analysis above, the cluster algorithm is the key step to find the cluster amount and its center in the zero-pole map. The threshold d_{th} is a key factor which can only determined by experimental statistics. Through many groups of experimental tests from real collected data, we get the statistics distribution curve of clustered zeros which are verified as true IMI by post-processing manually, as shown in Fig 12.

We give out the statistics figure in Fig.10 where zeros of PEF order with 4,6 and 8 are participating in the statistics. From the statistics we can conclude that majority of zeros have amplitude between 0.8 and 1.0, centered at about 0.92, so $d_{th} = 0.2$ is a proper value.

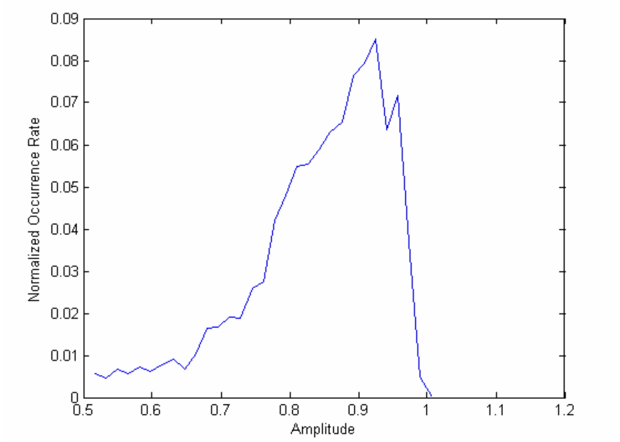

Fig.12 Amplitudes Statistics Distribution of Clustered Zeros

5 Conclusion

A viable algorithm for temporal IMI detection from OTHR data has been developed and demonstrated in this paper, where the IMI phase spectrum is regarded as complex sinusoid and modeled by means of AR model. The sinusoid frequency corresponding to IMI position is then estimated through the zeros of PEF transfer function. Experimental data from real OTHR system are used to verify its performance, and the zeros perfectly indicate the potential IMIs, including the amount and their respective position. Experiments also prove that clutter suppression brings little impact on the results even the simplest processing. Consequently, this proposed algorithm can work soundly and efficiently.

Further work will focus on the IMI suppression based on the position estimation provided by this proposed algorithm, as well as a proper method for selection on PEF order.

References:

[1] J.M. Headrick, M.I. Skolnik, Over-the-Horizon radar in the HF band, *Proceedings of the IEEE*, Vol 62, Issue 6, June 1974, 664-673

[2] Jr.J.Maresca, J.Barnum, Theoretical limitation of the sea on the detection of low Doppler targets by over-the-horizon radar, *IEEE Transactions on Antennas and Propagation*, Vol 30, Sep 1982, 837 - 845

[3] Gill, etc, The Effect of Bistatic Scattering Angle on the High Frequency Radar Cross Sections of the Ocean Surface, *IEEE Geoscience and Remote Sensing Letters*, Vol. 5, No. 2, 2008, 143-146.

[4] E. Serrano, Radar: signal analysis during operation time using wavelets, *Proceedings of the 2nd WSEAS International Conference on Wavelets Theory and Applications in Applied Mathematics, Signal Processing and Modern Science*, Istanbul, Turkey, 2008, 152-156,

[5] R. H. Khan, etc, Experimental results from a long-range HF ground wave coastal surveillance radar, *IEEE National Radar Conference*, Boston,USA, May 20.1993, 20-22

[6] V. Bazin, etc, Nostradamus: An OTH Radar, IEEE Aerospace and Electronic Systems Magazine, vol.21, 2006, 3-11

[7] G.A.Fabrizio, A.B.Gershman, M.D.Turley, Non-Stationary Interference Cancellation in HF Surface Wave Radar, *Proceedings of the International Radar Conference 2003*, Sept. 2003, 672-677

[8] G.A.Fabrizio, A.B.Gershman, M.D.Turley, Robust adaptive beamforming for HF surface wave over-the-horizon radar, *IEEE Trans. on AES*, vol 40, April 2004, 510-525

[9] R. H. Khan, Ocean-clutter model for high-frequency radar, *IEEE journal of oceanic engineering*, Vol.~16, 1991,181-188

[10] Wei Min, etc., Meteor Trail Interference Model in HF Environment,*2006 International Conference on Communication, Circuits and Systems Proceedings*, June 2006, 624-628

[11] Liu Tao, etc, Fractal Features and Detection of Meteor Interference in OTHR, *2006 CIE International Conference on Radar*, Shanghai, China, 16-19 Oct. 2006, 1-5.

[12] Liu Tao, etc, An Effective Fractal Algorithm for Meteor Interference Detection in OTHR, *2006 China-Japan Joint Microwave Conference Proceeding*, Chengdu, China, 2006, 727-731

[13] J.R.Barnum, E.E.Simpson, Over-the-Horizon Radar Sensitivity Enhancement by impulsive noise excision, *IEEE National Radar Conference*, 1997, 252-256

[14] Guo Xin, etc, Development of sky wave over-the-horizon radar, *ACTA Aeronautica et Astronautica Sinica*, vol.23, 2002, 495-500

[15] LIU Tao, GONG Yao-huan, CHEN Xiao-xu, Signal source of impulsive interference platform in OTHR, *Chinese Journal of Scientific Instrument*, Adopted

[16] M.Turley, Impulsive Noise Rejection in HF Radar Using a Linear Prediction Technique, Proceedings of the International Radar Conference, 3-5 Sept. 2003,358-362

[17] G.A.Fabrizio, A.Farina, M.D.Turley, Spatial Adaptive Subspace Detection in OTH radar, *IEEE Trans. on AES*, vol 39, Oct. 2003, 1407-1428

[18] G.A.Fabrizio, D.A.Gray, M.D.Turley, Parametric Localisation of Space-Time Distributed sources, *2000 IEEE International Conference on Acoustics, Speech, and Signal Processing*, Vol 5, 2000, 3097-3100

[19] G.A.Fabrizio, G.J.Frazer, M.D.Turley, STAP for Clutter and Interference Cancellation in a HF Radar System, *ICASSP 2006 Proceedings, Toulouse*, Vol 4, May 2006,1033-1036

[20] Huang Liang, etc, Suppressing instantaneous interference of high frequency ground wave radar, *Chinese Journal of Radio Science*, vol. 19, 2004, 166-170

[21] Xing Meng-dao, etc, Transient Interference Excision in OTHR, *ACTA ELECTRONICA SINICA*, vol.30, 2002, 823-826

[22] B.Root, HF radar ship detection through clutter cancellation, *Proceedings of the 1998 IEEE Radar Conference*, May 1998, 281-286

[23] S. D. Stearns, R. A. David, *Signal Processing Algorithms* , Englewood Cliffs, NJ: Prentice-Hall, 1988.

[24] B. Widrow, S. D. Stearns, *Adaptive Signal Processing* , Englewood Cliffs, NJ: Prentice-Hall, 1985.

[25] Richard O.Duda, Peter E.Hart, David G.Stork, *Pattern Classification, Second Edition*, John Wiley & sons, Inc., 2000